**Biophysical Journal, Volume 99**

## Supporting Material

# *In Vitro* Fracture Testing of Sub-micron Diameter Collagen Fibril Specimens

Zhilei Liu Shen, Mohammad Reza Dodge, Harold Kahn, Roberto Ballarini, Steven J. Eppell

## SUPPORTING MATERIAL

### S1: Sea Cucumber Type I Collagen Fibrils

Type I collagen fibrils were isolated from the dermis of sea cucumber, *Cucumaria frondosa* (1). This structure has a length of several dozen microns, a diameter of 10–500 nm, and is obtainable as an isolated fibril. Sea cucumber fibrils are similar to those found in vertebrates in that they have the same length, assemble with the same axial repeat period (~67 nm), and possess the same gap/overlap ratio (2) and cross-linking chemistry (3). However, the habit of echinoderm fibrils is spindle-shaped rather than cylindrical, as found in mammals. In addition, the collagen amino and carboxy termini are arranged in a bipolar manner, with their center of symmetry at the middle of the long axis of the spindle, rather than monopolar as found in mammals. Because the length of fibrils tested in this work (~10 μm) is a small fraction of the overall length, the shape can be approximated as cylindrical; it is likely that the center of the fibril was not in the gauge region thus we probably tested a monopolar array of collagen molecules. In addition, the echinoderm Type I collagen molecule is an α1 trimer (1) as opposed to the $(\alpha1)_2(\alpha2)_1$ heteromer found in mammals. Perhaps the biggest difference between echinoderm collagen fibrils and those of other animals is at the systemic level (2, 4). Echinoderms have the ability to change the mechanical properties of their collagen fibrillar networks over physiologically relevant timescales using a mechanism that is interfaced with their neural systems. However, the set of molecules relevant to this process is not present in the structure we studied. Collagen cross-link density is expected to play a strong role in the mechanics of the fibril as based on both modeling (5) and straightforward physical arguments. There are relatively few published data on the degree of cross-linking in sea cucumber collagen (4, 6, 7). Because our source of fibrils was highly dispersed in solution, it was not possible to determine the degree of cross-linking in the tested samples with direct spectroscopic measurements.

### S2: Calculating the *in vitro* cross-sectional areas of collagen fibril specimens from the *in vacuo* SEM measurements

We expected fibril specimens to dehydrate in the SEM vacuum chamber resulting in aberrantly small cross-sectional area measurements. To account for differences between the *in vacuo* measured cross-sectional area and the *in vitro* cross-sectional area during fracture testing, we performed a separate calibration experiment. Nine fibril specimens were extracted from solution and fixed to MEMS devices with epoxy droplets following the same protocol described in the "Sample Preparation" section. After the epoxy set overnight, ~ 100 μL 1× PBS buffer was added to the MEMS devices. The specimens were allowed to rehydrate by storing the MEMS devices at 4 °C for over 24 hours. The specimens were imaged in liquid using tapping mode AFM (Multimode Nanoscope IV, Veeco Instruments Inc., Plainview, NY). The specimens were then rinsed with deionized water to remove buffer salts, left at ambient air conditions overnight and then placed in the SEM vacuum chamber attaining the final state of dehydration that existed prior to imaging during our mechanical testing experiments.

For the AFM images obtained *in vitro* using tapping mode AFM, we measured heights and half-height widths at 10 different locations on each specimen. For the SEM images obtained *in vacuo*, we measured the widths of specimens at both 0° and 45° tilt angles, and at least 5 axial locations

on each specimen at each angle. Assuming the shape of the flattened specimen on the fixed pad is a half-ellipse, the *in vacuo* height of the specimen was calculated from the widths at 0° and 45° tilt angles.

Using 9 fibril specimens, we determined a ratio of *in vitro* cross-sectional area to *in vacuo* cross-sectional area of 4.85 ± 1.88 (mean ± SD; range, 2.06-7.59; n = 9). For the fibril specimens tested in the fracture tests, the *in vacuo* cross-sectional areas ( $A_{in\ vacuo}$ ) were calculated based on the widths and heights measured from the SEM images. Then, the *in vitro* cross-sectional areas were obtained by multiplying $A_{in\ vacuo}$ with the ratio of 4.85.

**S3: Calculating the ratio of cross-sectional area in the gauge region to that on the fixed pad**

All the mechanical properties reported in this manuscript were calculated using the cross-sectional area measured from the portion of specimen on the fixed pad. However, the portion of specimen in the gauge region (i.e. the actual tested specimen) may have a different cross-sectional area than the portion of specimen on the fixed pad (where the AFM and SEM images were taken) because the fibril diameter is known to vary along the fibril length (2). To investigate this, we fixed five fibril specimens onto MEMS devices and measured the cross-sectional areas both in the gauge region and on the fixed pad using SEM. We determined a ratio of cross-sectional area in the gauge region to that on the fixed pad to be 0.69 ± 0.42 (mean ± SD; range, 0.19-1.26; n = 5).

Some mechanical properties, such as strain at the initiation of damage and fracture strain, are not affected by this ratio. However, other mechanical properties, such as elastic modulus, strength at the initiation of damage, fracture strength, and work of fracture, are because the stress is inversely proportional to the cross-sectional area. Thus elastic modulus, strength at the initiation of damage, fracture strength, and work of fracture of collagen fibril specimens may be in the range of 0.79-5.26 times of what were reported in the manuscript. Fig. S2 shows the possible range one stress-strain curve may fall in.

**S4: Uncertainty analysis**

The uncertainty of DIC was determined using a method similar to the one used by Naraghi *et al.* (8). A MEMS device was mounted on a piezo stage (P-517, PI (Physik Instrumente) L.P., Auburn, MA). The piezo stage was driven at a displacement rate of 20 nm/sec and optical images of the MEMS device were taken every two seconds using the same microscope/digital camera set-up as in the fracture test. Thus the nominal displacement of the piezo stage between two adjacent images (step size) is 40 nm. The nominal displacement of the piezo stage during the whole calibration was then calculated from this 40 nm step size and the image number, and it is represented by the straight line in Fig. S3. The rigid body displacements of three parts of the MEMS devices, including the fixed pad, the movable pad, and the force gauge pad, were monitored. Since no probe was placed in the pushing hole, all three parts moved together with the piezo stage and their rigid body displacements determined by DIC should be the same as the displacement of the piezo stage. The experimental displacement of the piezo stage determined by DIC was plotted as a function of the image number ('×' in Fig. S3), which matched very well with the nominal displacement of the piezo stage (the straight line in Fig. S3). The maximum

difference between them was ~ 38 nm. Thus the uncertainty in the relative motion between two parts of the MEMS device (e.g. between the fixed pad and the movable pad) is $38 \times \sqrt{2} \approx 54$ nm by virtue of error propagation. This is similar to the 65 nm uncertainty obtained by Naraghi *et al.* (8) considering that they used a 50× air objective lens while we used a 60× water immersion lens.

The uncertainty in the engineering strain ( $\varepsilon = \frac{d}{l_0}$ ) is

$$\Delta\varepsilon = \sqrt{(\frac{\partial\varepsilon}{\partial d}\Delta d)^2 + (\frac{\partial\varepsilon}{\partial l_0}\Delta l_0)^2} = \sqrt{(\frac{1}{l_0}\Delta d)^2 + (\frac{d}{l_0^{\,2}}\Delta l_0)^2},$$

where $\Delta d$ is the uncertainty in the measured change in length, which is the same as the uncertainty in the displacement determined by DIC (~54 nm), and $\Delta l_0$ is the uncertainty in the initial gauge length measured from SEM images.

The uncertainty in the nominal stress ( $\sigma = \frac{F}{A_o} = \frac{4F}{\pi D_0^{\,2}}$ ) is

$$\Delta\sigma = \sqrt{(\frac{\partial\sigma}{\partial F}\Delta F)^2 + (\frac{\partial\sigma}{\partial A_0}\Delta A_0)^2} = \sqrt{(\frac{1}{A_0}\Delta F)^2 + (\frac{F}{A_0^{\,2}}\Delta A_0)^2}$$

$$= \sqrt{(\frac{\partial\sigma}{\partial F}\Delta F)^2 + (\frac{\partial\sigma}{\partial D_0}\Delta D_0)^2} = \sqrt{(\frac{4}{\pi D_0^{\,2}}\Delta F)^2 + (\frac{8F}{\pi D_0^{\,3}}\Delta D_0)^2},$$

where $\Delta F$ , $\Delta A_0$ , and $\Delta D_0$ are the uncertainties in the force measured from the force gauge, the initial cross-sectional area, and the initial diameter measured from SEM images, respectively.

**S5: The spread in the mechanical properties**

The spread in the mechanical properties reported above is relatively large. This is partly because a limited number of fibril specimens were tested due to the difficulty in setting up the experiments. Furthermore, spread in the values likely comes from both systematic experimental error and intrinsic sample variability. The systematic error arises mainly from calculating the cross-sectional area of the fibril, including the conversion from *in vacuo* to *in vitro* areas and the conversion from AFM and SEM measurements made on the surface of the fixed pad to the actual SEM measurements made on the unsupported portion of the specimen in the gauge region (see the supporting material section S2 and S3). The intrinsic sample variability is possibly due to different cross-link density, different collagen molecule packing within the fibril, different fibril geometry, and different levels of hydroxylation of amino acids. Experimental determination of cross-link density on individual fibrils was not possible. However, molecular dynamic simulation study showed that the mechanical response changed with cross-link density (5). With low cross-link density, the fibril has an initial linear region followed by a ductile yield region and can dissipate a lot of energy; with high cross-link density, the fibril shows an initial linear region followed by a second, stiffer elastic region and becomes brittle. The yield strength and fracture strength increase with increasing cross-link density. For the fibril geometry, we previously demonstrated that the yield strength decreased with increasing fibril volume (9). However, we did not find a similar correlation for the *in vitro* study probably due to the error in the cross-

sectional area. Finally, it is likely that degrees of post-translational modification (ex. hydroxylation of prolines and lysines), were not uniform across the different fibrils. This would alter the hydrogen bonding interactions among the molecules in the systems and would be expected to affect the measured mechanical properties.

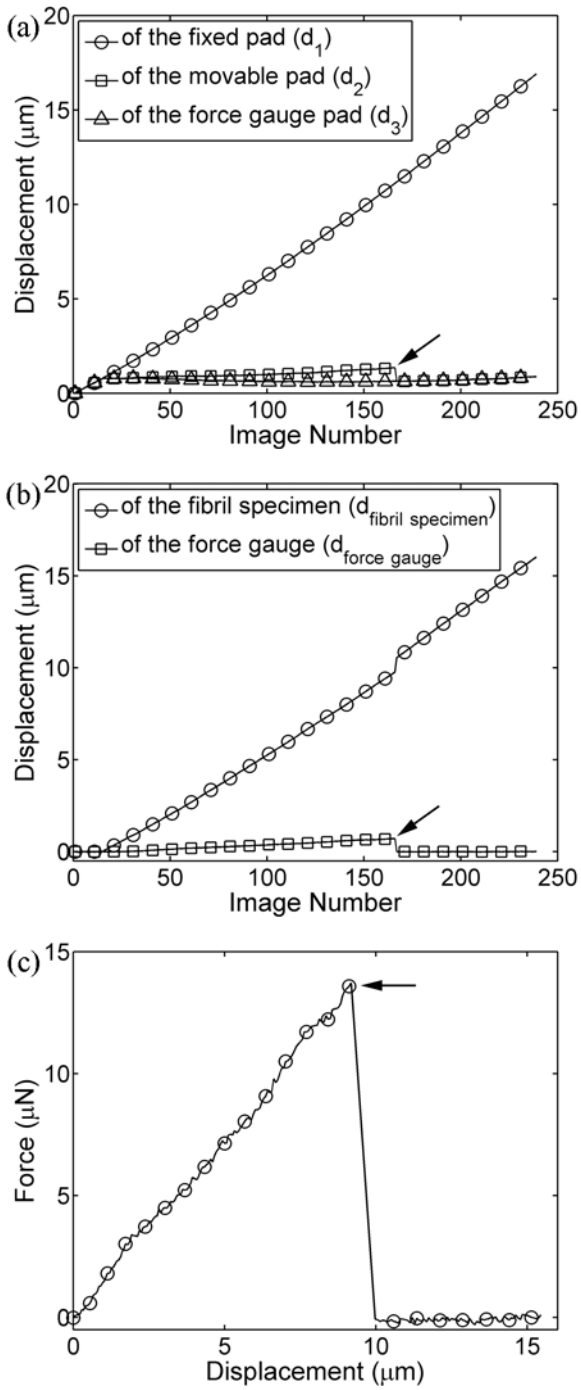


**FIGURE S1** (a) Displacements of the fixed pad ($d_1$, '○'), the movable pad ($d_2$, '□'), and the force gauge pad ($d_3$, 'Δ') obtained by DIC; (b) displacements of the fibril specimen ($d_{fibril\ specimen}$, '○') and the force gauge ($d_{force\ gauge}$, '□'); (c) force-displacement curve of the collagen fibril specimen. The arrows indicate where the specimen fractured. For the sake of clarity, the symbols are shown every ten data points.

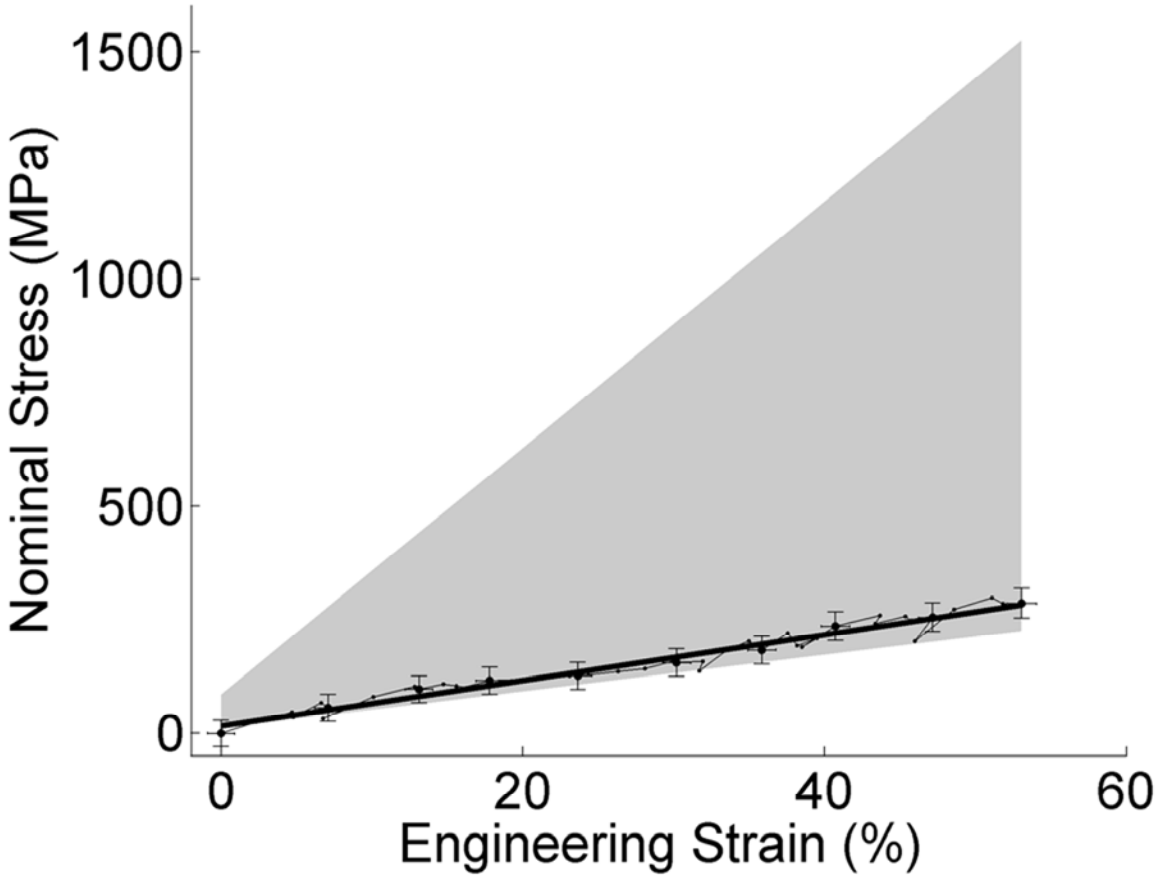


**FIGURE S2** Considering the ratio of cross-sectional area in the gauge region to that on the fixed pad is in the range of 0.19-1.26, the stress-strain curve of the fibril specimen shown in Fig. 3a may be anywhere in the shadowed area.

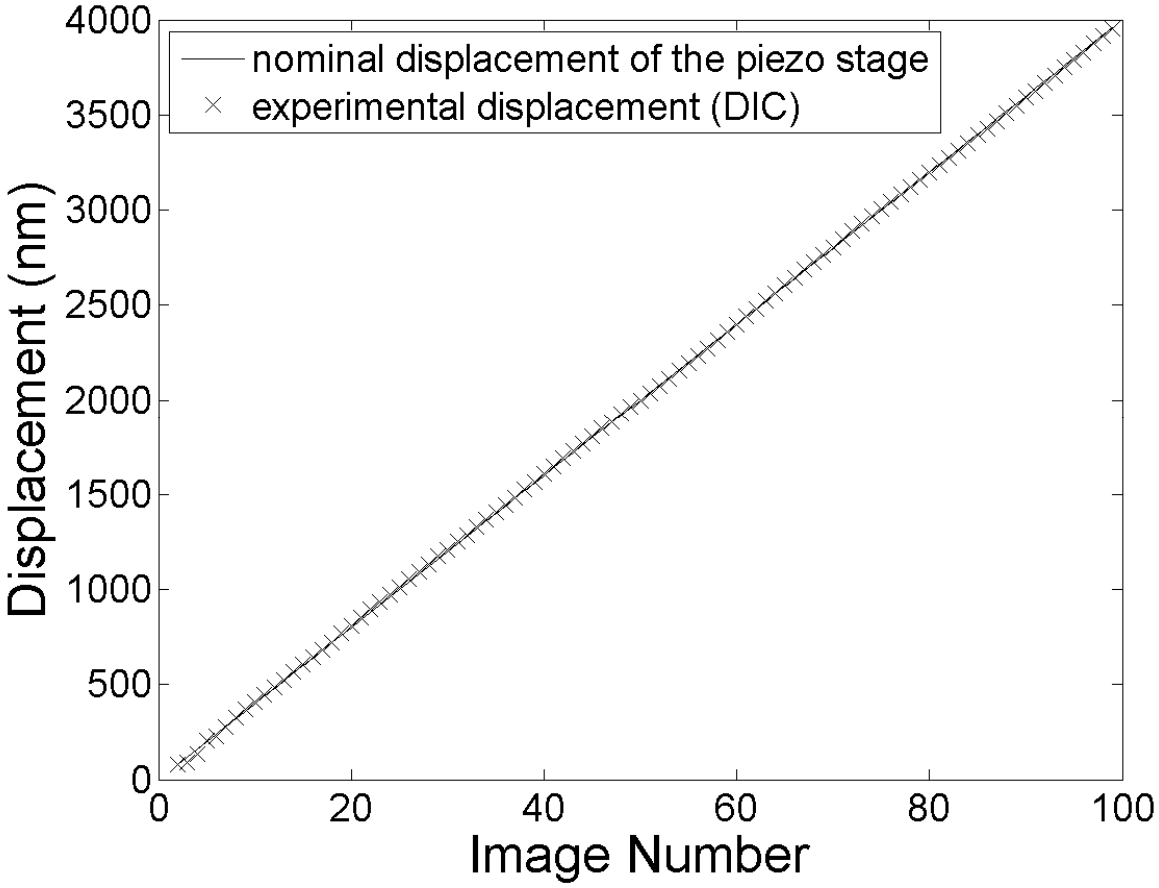


**FIGURE S3** Comparison of the experimental displacement of a piezo stage determined by DIC ('×') with its nominal displacement (the straight line) during a calibration with a step size of 40 nm.

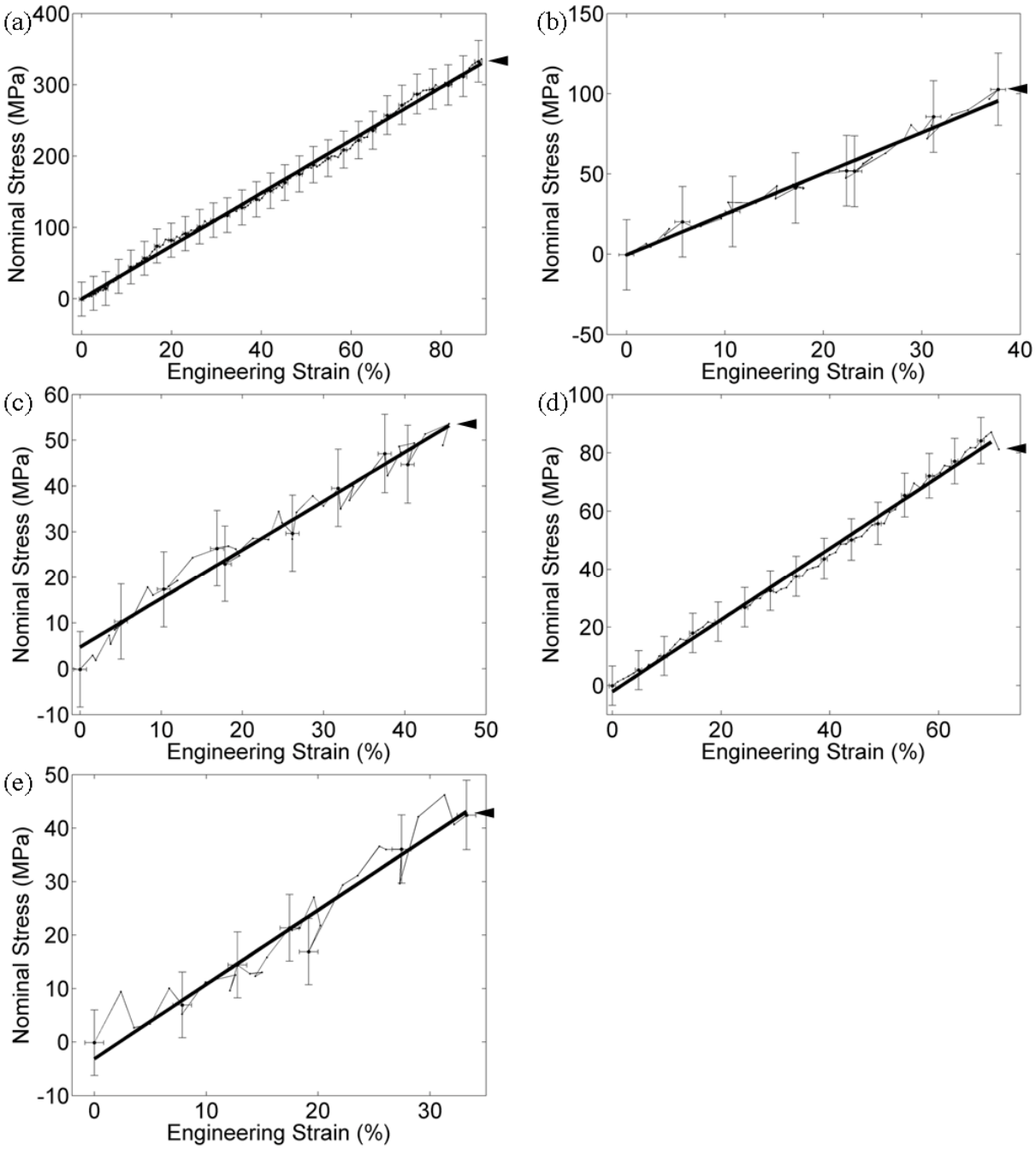


**FIGURE S4** Stress-strain curves of the other five fibril specimens in Group I. Each of them showed a relatively linear region all the way to brittle fracture. For the sake of clarity, the error bars are shown every five data points. The thick solid lines represent the least-squares fits to relatively linear regions. The fracture point is defined as the point where the stress dropped back to zero (indicated by solid arrowheads).

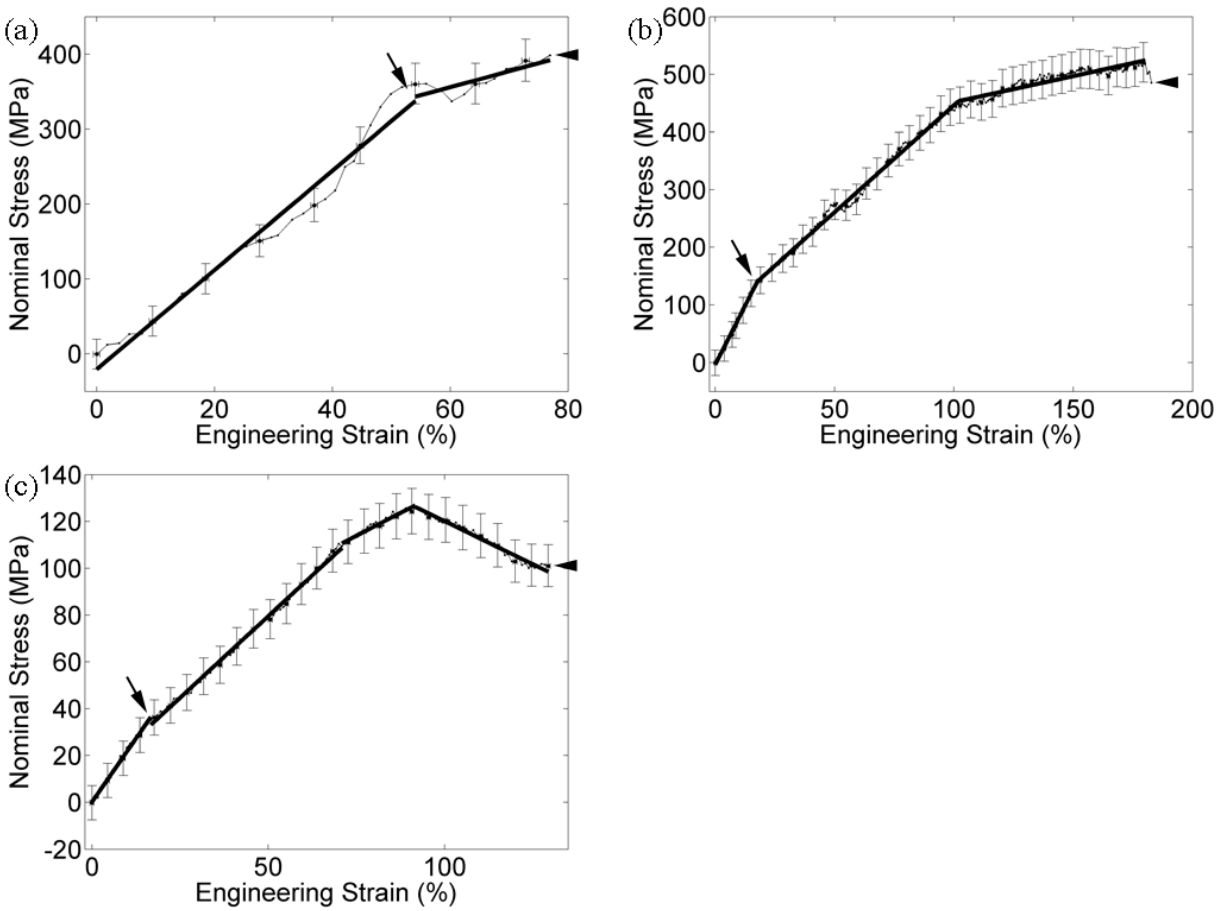


**FIGURE S5** Stress-strain curves of the other three fibril specimens in Group II. Each of them showed multiple linear regions prior to brittle fracture. For the sake of clarity, the error bars are shown every five data points. The thick solid lines represent the least-squares fits to relatively linear regions. The fracture point is defined as the point where the stress dropped back to zero (indicated by solid arrowheads). The initiation of damage is defined as the intersection of the first two fitted lines (indicated by arrows).

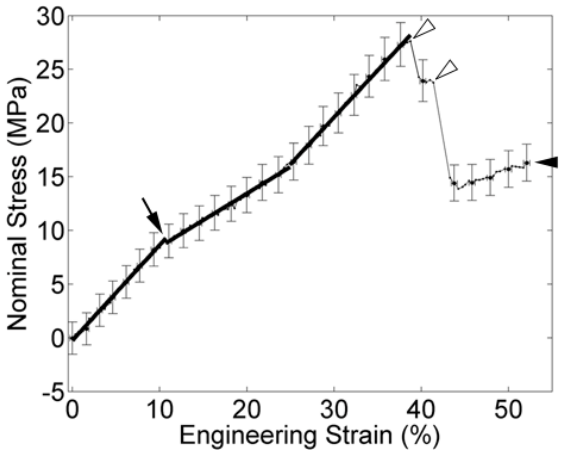


**FIGURE S6** Stress-strain curves of the other collagen fibril specimen in Group III. It showed multiple linear regions followed by a step-wise graceful fracture region. For the sake of clarity, the error bars are shown every five data points. The thick solid lines represent the least-squares fits to relatively linear regions. The fracture point is defined as the point where the stress dropped back to zero (indicated by solid arrowheads). The initiation of damage is defined as the intersection of the first two fitted lines (indicated by arrows). Multiple drops in the graceful fracture region (indicated by hollow arrowheads) were observed, suggesting multiple partial fractures before the complete fracture (indicated by solid arrowhead).

**TABLE S1** Comparison of the diameter, elastic modulus and fracture strength/strain of collagen fibril specimens in the current study with those of collagen fibril bundles, fascicles, and tendons obtained via experiments in the literature.

| Technique | Specimens | Diameter (μm) | E (MPa) | $\sigma_{max}$ (MPa) | $\varepsilon_{max}$ (%) |
|---|---|---|---|---|---|
| Tensile test using MEMS * | sea cucumber dermis fibrils | 0.21-0.45 | 470 ± 410 | 230 ± 160 | 80 ± 44 |
| Tensile test using micro-tensile test system (10) | Rabbit patellar tender fibril bundles | 1.01 ± 0.06 | 54.3 ± 25.1 | 8.5 ± 2.6 | 21.6 ± 3.0 |
| Tensile test using micro-tensile test system and SAXS (11) | Rat tail tendon fibril bundles | 90 ± 20 | 14 | 100 | 13 |
| Tensile test using confocal microscopy and fluorescently labeled tenocyte (12) | Rat tail tendon fascicles | 100 | 662.7 ± 167 | 47.1 ± 8.4 | 14.4 (9.5-16.2) |
| Tensile test using micro-tensile test system (13) | Mouse tail tendon fascicles | 122.5 ± 69.4 | 423.5 ± 76.6 | 26.4 ± 1.9 | 11.1 ± 1.8 |
| Tensile test using micro-tensile test system (14) | Rabbit patellar tendon fascicles | 300 | 216 ± 68 | 17.2 ± 4.1 | 10.9 ± 1.6 |
| Tensile test using micro-tensile test system (14) | Rabbit patellar tendon | 3000 | 732 ± 200 | 40.5 ± 4.3 | 6.1 ± 1.0 |

* Present work.

**REFERENCES**


1. Trotter, J. A., G. Lyons-Levy, F. A. Thurmond, and T. J. Koob. 1995. Covalent composition of collagen fibrils from the dermis of the sea cucumber, Cucumaria frondosa, a tissue with mutable mechanical properties. Comp Biochem Physiol A Physiol 112:463-478.
2. Trotter, J. A., F. A. Thurmond, and T. J. Koob. 1994. Molecular structure and functional morphology of echinoderm collagen fibrils. Cell Tissue Res 275:451-458.
3. Butler, E., J. Hardin, and S. Benson. 1987. The role of lysyl oxidase and collagen crosslinking during sea urchin development. Exp Cell Res 173:174-182.
4. Thurmond, F. A., and J. A. Trotter. 1996. Morphology and biomechanics of the microfibrillar network of sea cucumber dermis. J Exp Biol 199:1817-1828.
5. Buehler, M. J. 2008. Nanomechanics of collagen fibrils under varying cross-link densities: Atomistic and continuum studies. J Mech Behav Biomed Mater 1:59-67.
6. Eyre, D. R., and M. J. Glimcher. 1973. Evidence for glycosylated crosslinks in body-wall collagen of the sea cucumber, Thyome briareus. Proc Soc Exp Biol Med 144:400-403.
7. Thurmond, F. A., T. J. Koob, J. M. Bowness, and J. A. Trotter. 1997. Partial biochemical and immunologic characterization of fibrillin microfibrils from sea cucumber dermis. Connect Tissue Res 36:211-222.
8. Naraghi, M., I. Chasiotis, H. Kahn, Y. Wen, and Y. Dzenis. 2007. Novel method for mechanical characterization of polymeric nanofibers. Rev Sci Instrum 78:085108.
9. Shen, Z. L., M. R. Dodge, H. Kahn, R. Ballarini, and S. J. Eppell. 2008. Stress-strain experiments on individual collagen fibrils. Biophys J 95:3956-3963.
10. Miyazaki, H., and K. Hayashi. 1999. Tensile Tests of Collagen Fibers Obtained from the Rabbit Patellar Tendon. Biomed Microdevices 2:151-157.
11. Misof, K., G. Rapp, and P. Fratzl. 1997. A new molecular model for collagen elasticity based on synchrotron x-ray scattering evidence. Biophysical Journal 72:1376-1381.
12. Screen, H. R., D. A. Lee, D. L. Bader, and J. C. Shelton. 2004. An investigation into the effects of the hierarchical structure of tendon fascicles on micromechanical properties. Proc Inst Mech Eng [H] 218:109-119.
13. Derwin, K. A., and L. J. Soslowsky. 1999. A quantitative investigation of structure-function relationships in a tendon fascicle model. J Biomech Eng 121:598-604.
14. Yamamoto, E., K. Hayashi, and N. Yamamoto. 1999. Mechanical properties of collagen fascicles from the rabbit patellar tendon. J Biomech Eng 121:124-131.